

Quantum dot-based high-fidelity universal quantum gates in noisy environment

Yash Tiwari, Aditya Dev, Vishvendra Singh Poonia

Abstract—Quantum dot-based spin qubit realization is one of the most promising quantum computing systems owing to its integrability with classical computation hardware and its versatility in realizing qubits and quantum gates. In this work, we investigate a quantum dot-based universal set of quantum gates (single qubit gates and the Toffoli gate) in the presence of hyperfine fluctuation noise and phononic charge noise. We model the spin dynamics and noise processes in the NOT gate, Hadamard gate and the Toffoli gate using the Lindblad master equation formalism to estimate the operating ranges of the external static and ac magnetic fields to achieve high fidelity operation of these gates in a noisy environment. In addition, the generality of the framework proposed in this paper enables modeling of larger quantum processors based on spin qubits in realistic conditions.

Index Terms—Quantum dots, spin qubits, dephasing, universal quantum gates, Hadamard gate, Toffoli gate

I. INTRODUCTION

In 1998, Loss and DiVincenzo proposed a quantum dot based implementation of quantum computation that used electron spin as a qubit [1]. Since then, tremendous progress has been made on quantum dot based spin qubits [2]–[11]. To implement an arbitrary quantum operation, we need to have a set of ‘universal’ quantum gates. There exist many such sets that can act as universal quantum gates according to Solovay-Kitaev theorem [12], [13]. However, qubits interact with the environment, which affects the gate implementation and deteriorates their fidelity. For example, in a GaAs QD system, we observe interactions with i) spin of surrounding nuclei and ii) phonons [14]–[21]. Similar is the case with Si quantum dot based qubits. Both of these are the primary sources of decoherence in the qubits. The spin of the nuclei surrounding the confined electron in the quantum dot exhibits a normalized magnetic field distribution. This magnetic field interacts with the spin of a confined electron introducing hyperfine interaction (HFI) noise in the system. The interaction with phonons essentially captures the charge noise due to lattice vibrations. It is mediated by the spin-orbit interaction (SOI) [22], [23]. Generally, spin qubits cannot be directly affected by electric field fluctuations. Spin-orbit interaction (SOI) mixes the spin states with the orbital (electron cloud) state making the system susceptible to electrostatic fluctuations [15]. As pointed out

earlier as well, the phonon interaction is the dominant source of charge fluctuation in the quantum dot environment that we have taken in our study. It has been observed that HFI noise is dominant at the low external static magnetic field (low energy gap), and phonon noise is dominant at the high value of static magnetic field (high energy gap) [15]. The silicon-based spin qubits are relatively free from hyperfine interactions and therefore they are well suited for spin-based quantum computing. However, they suffer from a problem inherent to their electronic structure. The conduction band minima of silicon have six-fold degeneracy providing an uncontrolled degree of freedom for electrons that are used to define qubits and it may cause relaxation and dephasing in the qubit state [24], [25].

In this work, we present a general framework to model the spin dynamics of the universal set of quantum gates in noisy environment. We examine the fidelity of the gates and find out the parameter regime to achieve the high-fidelity ($\geq 98\%$) gate operations. One of the most popular universal gate sets is the combination of Toffoli gate and Hadamard gate [26], [27]. We identify a common parameter regime where both gate operations show high fidelity. The proposed framework is general in nature and can be extended to more qubits and larger quantum processors based on spin qubits. This would also allow one to include quantum control techniques used to enhance the gate fidelity further and reduce the error correction overhead. In this framework, we use Lindblad master equation formalism to model the spin dynamics and decoherence due to noise in the spin system.

The manuscript has been organized as follows: Section II discusses the modeling and numerical methodology followed for the analysis. Section III discusses the result for single qubit quantum gates. In addition to the Hadamard gate operation, we also discuss NOT gate in detail in this section. Section IV discusses the results for the three-qubit Toffoli gate. Finally, we conclude the paper with a discussion about extending the framework and identifying the future directions.

II. METHODOLOGY

In this section, we discuss the modeling of qubit spin dynamics and noise processes therein. We use the Lindblad operator equation for this purpose that can be written as (Eq. 1):

$$\frac{d\rho(t)}{dt} = L_0 + L_D. \quad (1)$$

$$L_0 = -\frac{i[H(t), \rho(t)]}{\hbar}. \quad (2)$$

This work is supported by the Science and Engineering Research Board, Department of Science and Technology (DST), India, with Grants No. CRG/2021/007060 and No. DST/INSPIRE/04/2018/000023.

Vishvendra Singh Poonia and Yash Tiwari are with the Department of Electronics and Communication Engineering, Indian Institute of Technology, Roorkee, India. (Email: vishvendra@ece.iitr.ac.in)

Aditya Dev is with the Department of Physical Sciences, Indian Institute of Science Education and Research (IISER) Mohali.

A quantum system's coherent and non-coherent time evolution is observed due to L_0 and L_D , respectively. The general formulation of L_0 is given in Eq. 2, where $H(t)$ is the complete Hamiltonian of a closed system, $\rho(t)$ denotes quantum state at arbitrary time instant t . The non-coherent evolution operator L_D is described in Eq. 3.

$$L_D = \sum_n \frac{1}{2} \{ 2C_n \rho(t) C_n^\dagger - \rho(t) C_n^\dagger C_n - C_n^\dagger C_n \rho(t) \} \quad (3)$$

The C_n , in general, would be associated with a rate and an accompanying operator. C_n due to relaxation would have an operator of form $|w_j\rangle \langle w_k|$ where the energy relaxation would be happening from energy level w_k to w_j . The rate associated with the operator would be a function of the energy gap ($E_{w_j} - E_{w_k}$). Operator associated due to dephasing is of the form of σ_z , where σ_z is the Pauli-Z matrix. The rate associated with the dephasing is the inverse of T_2^* which is a material dependent parameter. In this work, we have used parameters corresponding to GaAs quantum dot system, however, the framework presented is quite general and applicable to other spin qubit systems including the ones based on Si quantum dots.

$$C_{i1} = \sqrt{\Upsilon_{jk}^+} |w_j\rangle \langle w_k| = \sqrt{\Upsilon e^{\frac{-\omega_{jk}^2}{2\delta E_{nuc}^2}} |w_j\rangle \langle w_k|} \quad (4)$$

$$C_{i2} = \sqrt{\Upsilon_{kj}^-} |w_k\rangle \langle w_j| = \sqrt{\Upsilon e^{\frac{-\omega_{kj}^2}{2\delta E_{nuc}^2} + \frac{\omega_{kj}}{T_k}} |w_k\rangle \langle w_j|} \quad (5)$$

$$C_{i3} = \sqrt{P_{jk}^+} |w_j\rangle \langle w_k| = \sqrt{P \left| \frac{\omega_{jk}^3 E_{jk}^2}{1 - e^{-\frac{\omega_{jk}}{T_k}}} \right| |w_j\rangle \langle w_k|} \quad (6)$$

$$C_{i4} = \sqrt{P_{kj}^-} |w_k\rangle \langle w_j| = \sqrt{P \left| \frac{\omega_{kj}^3 E_{kj}^2}{1 - e^{-\frac{\omega_{kj}}{T_k}}} \right| |w_k\rangle \langle w_j|} \quad (7)$$

Eq. 4 to Eq. 7 denote the relaxation operators in a spin qubit system. In Eq. 4 and Eq. 6, $w_{jk} > 0$ corresponds to positive transition (energy absorption) whereas in Eq. 5 and Eq. 7, $w_{kj} < 0$ corresponds to negative transition (energy emission). C_{i1} (Υ_{jk}^+) and C_{i2} (Υ_{kj}^-) are positive and negative relaxation operators (rates) due to HFI noise. Similarly, C_{i3} (P_{jk}^+) and C_{i4} (P_{kj}^-) are positive and negative relaxation operators (rates) due to phononic noise [28]. In C_{i1} and C_{i2} , $\delta E_{nuc} = 0.3 \mu\text{eV}$ for GaAs [14], [29]. The parameter δE_{nuc} is associated with the nuclear magnetic field (due to nuclear spin) experienced by the confined electron. Υ is the constant associated with relaxation due to hyperfine noise, in C_{i1} and C_{i2} . The temperature of the system is $T_k = 10 \mu\text{eV}$ (125mK). P is the constant associated with the relaxation operator due to phononic interactions, whereas E_{kj} corresponds to Zeeman split between the energy levels [15], [28]. The dephasing operator is given in Eq. 8 where the value of T_2^* is taken from an experiment [30].

$$C_5 = L_{Dephasing} = \sqrt{\frac{1}{2T_2^*}} \sigma_z \quad (8)$$

In order to assess the efficacy of the gate operations, we use 'state fidelity' as a quantifier. State fidelity between two states ρ and σ is defined in Eq. 9 where Tr is the trace of a matrix. We use the schematic shown in Fig. 1 to calculate the fidelity of a gate operation as a function of time where U is the gate matrix, $H(t)$ is the system hamiltonian, $\rho(t)$ is the state of the system and σ is output after multiplication with gate matrix U . σ remains constant with time. State fidelity also helps us to understand the effect of relaxation and dephasing on a gate operation.

$$F(\rho, \sigma) = \left(Tr \left(\sqrt{\sqrt{\rho} \sigma \sqrt{\rho}} \right) \right)^2 \quad (9)$$

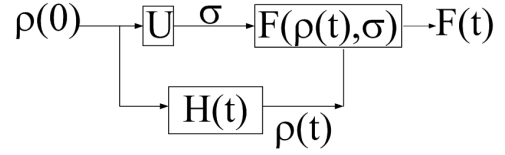


Fig. 1. Schematic used to calculate fidelity of quantum gates. U is the matrix corresponding to the gate operation, $H(t)$ is the system Hamiltonian. $\rho(t)$ is the state of the system and σ is the output after multiplication with gate matrix U . $F(t)$ is the state fidelity between ρ and σ .

In summary, the evolution of the qubit states and gate operation is modeled by the Lindblad master equation, and the fidelity of gate operations is evaluated through the schematic in Fig. 1. This analysis leads us to estimate the values of external parameters (dc and ac magnetic field values) to achieve high-fidelity gate operations. We employ this methodology on NOT gate, Hadamard gate, and Toffoli gate operations. We also study the effect of noise on the operations of all these gates.

III. SINGLE QUBIT QUANTUM GATES

The Hamiltonian of single-qubit gate operation (i.e. electron spin resonance (ESR)) is given by Eq. 10:

$$H(t) = g\mu B_{static} \sigma_z - g\mu B_{ac} (\cos(\omega t) \sigma_x - \sin(\omega t) \sigma_y) \quad (10)$$

where g is the gyromagnetic ratio, B_{static} and B_{ac} are the static and ac magnetic fields applied to the system. $\sigma_x, \sigma_y, \sigma_z$ are the Pauli matrices. When the initial state of the system can be defined as: $|\Phi(0)\rangle = a_0 |\uparrow\rangle + b_0 |\downarrow\rangle$, $|\Phi(t)\rangle$ is given as: $|\Phi(t)\rangle = a |\uparrow\rangle + b |\downarrow\rangle$ where

$$a = \left[a_0 \left(\cos \left(\frac{\omega_1 t}{2f} \right) - i f \frac{\omega - \omega_0}{\omega_1} \sin \left(\frac{\omega_1 t}{2f} \right) \right) + b_0 i f \sin \left(\frac{\omega_1 t}{2f} \right) \right] e^{i\omega t/2} \quad (11)$$

$$b = \left[b_0 \left(\cos \left(\frac{\omega_1 t}{2f} \right) - i f \frac{\omega - \omega_0}{\omega_1} \sin \left(\frac{\omega_1 t}{2f} \right) \right) + a_0 i f \sin \left(\frac{\omega_1 t}{2f} \right) \right] e^{-i\omega t/2} \quad (12)$$

$\omega_0 = g\mu B_{static}$, $\omega_1 = g\mu B_{ac}$ and ω is the applied frequency of ac magnetic field. f is defined by Eq. 13 as:

$$f = \sqrt{\frac{\omega_1^2}{(\omega - \omega_0)^2 + \omega_1}} \quad (13)$$

The value of f is unity at resonance, i.e. $\omega = \omega_0$ [31], [32]. When initial state is: $|\Phi(0)\rangle = |\uparrow\rangle$ ($a_0 = 1$ and $b_0 = 0$), $\Phi(t)$ will be given as:

$$|\Phi(t)\rangle = \left[\cos\left(\frac{\omega_1 t}{2}\right) e^{i\omega_0 t/2} |\uparrow\rangle + i \sin\left(\frac{\omega_1 t}{2}\right) e^{-i\omega_0 t/2} |\downarrow\rangle \right] \quad (14)$$

With this background, in two subsections, we will discuss the implementations of single qubit NOT and Hadamard gates.

A. NOT gate implementation

The NOT gate is implemented according to the scheme shown in Fig.1 where $U = [[0, 1], [1, 0]]$ and $H(t)$ would be same as Eq. 10. The $F(\rho(t), \sigma = |\downarrow\rangle)$ when $|\Phi(0)\rangle = |\uparrow\rangle$ is $\sin^2 \frac{\omega_1 t}{2}$ at resonant frequency $\omega = \omega_0$. We achieve $F = 1$ when $\frac{\omega_1 t}{2} = \frac{\pi}{2}$ at which NOT gate operation occurs. In Fig. 2(a), we have shown the fidelity (F) for a single qubit NOT operation as a function of B_{static} at low values of static magnetic field (few mT). The black (red) curve corresponds to the case when no noise (noise) is considered in the system. We take a threshold of 98% fidelity to find out the parameter regime where gate operation is achieved with high fidelity ($> 98\%$). The dotted lines correspond to $F = 0.98$. At values of $B_{static} \leq 7mT$, we observe that $F \leq 0.98$ due to hyperfine noise. In Fig.2(b), we observe that whether initially $\rho(0) = |\uparrow\rangle$ or $\rho(0) = |\downarrow\rangle$, the system show drop in F in a similar manner due to noise.

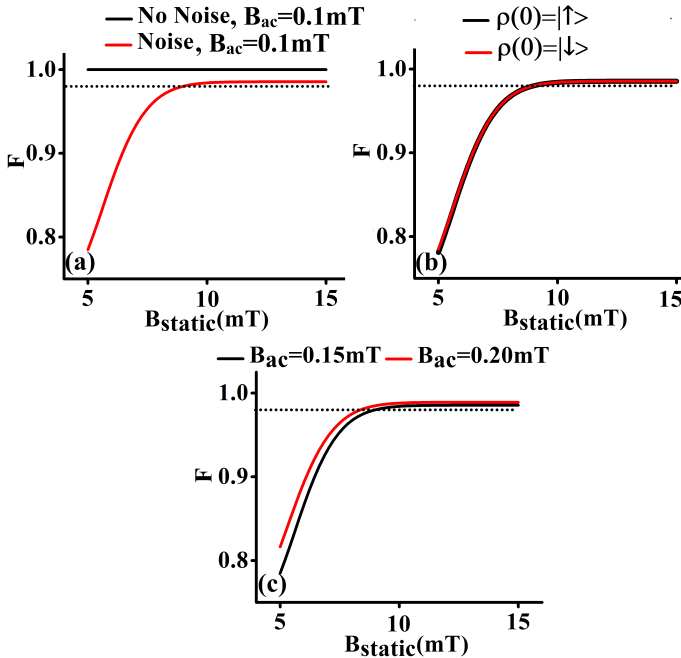


Fig. 2. (a) Fidelity vs B_{static} for NOT gate operation at $B_{ac} = 0.1mT$, when there is no noise (black), noise (red) in the system. (b) Fidelity comparison for NOT gate when $\rho(0) = |\uparrow\rangle$ (black) and $\rho(0) = |\downarrow\rangle$ (red) at $B_{ac} = 0.2mT$ (c) Fidelity vs B_{static} for two values of $B_{ac} = 0.15mT$ (black), $0.20mT$ (red). At high B_{ac} a much greater range of B_{static} can be used corresponding to $F \geq 0.98$ for NOT gate operation.

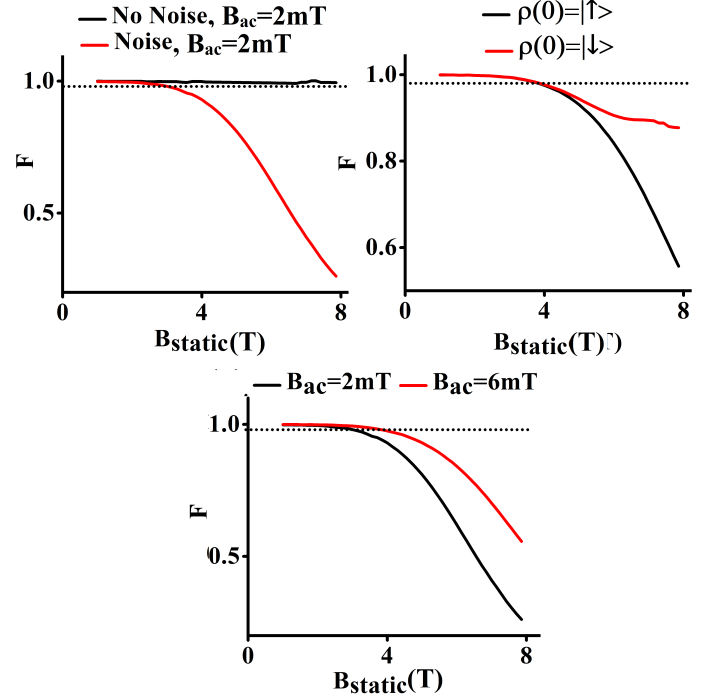


Fig. 3. (a) Fidelity vs B_{static} for NOT gate operation at $B_{ac} = 2mT$, when there is no noise (black), noise (red) in the system. (b) Fidelity comparison for NOT gate when $\rho(0) = |\uparrow\rangle$ (black) and $\rho(0) = |\downarrow\rangle$ (red) at $B_{ac} = 6mT$ (c) Fidelity vs B_{static} for two values of $B_{ac} = 2mT$ (black), $6mT$ (red). At high B_{ac} a much greater range of B_{static} can be used corresponding to $F \geq 0.98$ for NOT gate operation.

In Fig.2(c), we observe that as the ac field (B_{ac}) increases, B_{static} at which $F \geq 0.98$ decreases, thus increasing the working range of B_{static} . We also define a quantity called B_F which is the B_{static} at which system $F = 0.98$ with noise. A curve correlating B_F with B_{ac} has been examined in Ref. [33].

In Fig.3(a), we show F for a single qubit NOT gate operation as a function of B_{static} at high values of static magnetic field (few Tesla). The black (red) curve corresponds to the case when no noise (noise) is considered in the system. At values of $B_{static} \geq 3T$, we observe a fall in F due to phononic noise. In Fig. 3(b), we observe that till $F = 0.98$ threshold, $\rho(0) = |\uparrow\rangle$ and $\rho(0) = |\downarrow\rangle$ behave similarly. However, at extremely high B_{static} and with $\rho(0) = |\downarrow\rangle$, the system F decays slower compared to the case when $\rho(0) = |\uparrow\rangle$ due to noise. In Fig.3(c), as the ac field B_{ac} increases, B_F also increases. Thus increasing the working range of B_{static} .

B. Hadamard gate implementation

The Hadamard gate is implemented according to Fig. 1 with $U = \frac{1}{\sqrt{2}}[[1, 1], [1, -1]]$ and H would be same as Eq. 10. The $F(\rho(t), \sigma = \frac{1}{\sqrt{2}}(|\uparrow\rangle + |\downarrow\rangle))$ when $|\Phi(0)\rangle = |\uparrow\rangle$ is $1 + \sin(\omega_0 t) \sin(\omega_1 t)$ at resonant frequency $\omega = \omega_0$. We achieve $F = 1$ when either $\omega_0 t = n\pi$ or $\omega_1 t = m\pi$ or both (where n, m are integers). At this instance, the Hadamard gate operation takes place.

In Fig. 4(a), we have shown F for a single qubit Hadamard gate operation as a function of B_{static} at low values of static

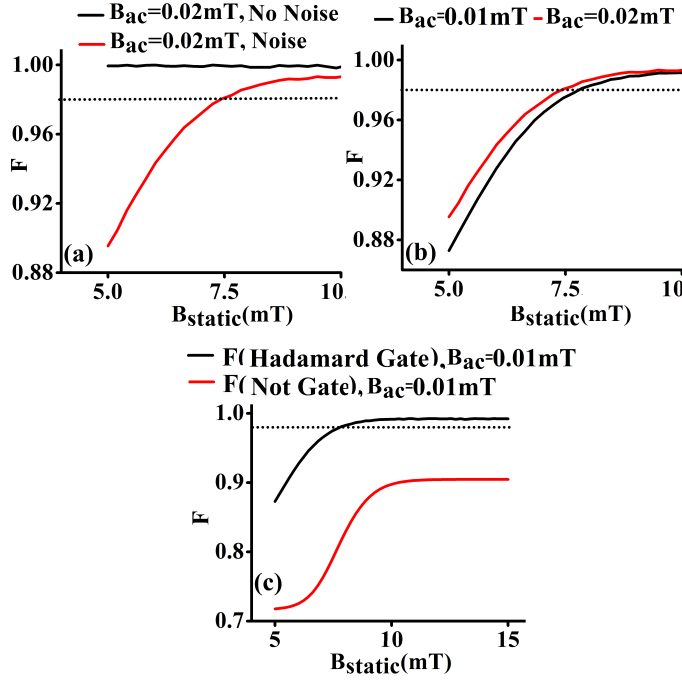


Fig. 4. (a) Fidelity vs B_{static} for Hadamard gate at $B_{ac} = 0.02\text{mT}$, when there is no noise (black), noise (red) in the system. (b) Fidelity vs B_{static} for two values of $B_{ac} = 0.01\text{mT}$ (black), 0.02mT (red). At high B_{ac} a much greater range of B_{static} can be used corresponding to $F \geq 0.98$ for Hadamard gate operation. (c) Fidelity comparison for NOT gate and Hadamard gate operation at $B_{ac} = 0.01\text{mT}$.

magnetic field (few mT). The black (red) curve corresponds to the case when no noise (noise) is considered in the system. The dotted lines correspond to $F = 0.98$. Both cases are taken at $B_{ac} = 0.02\text{mT}$. At low values of B_{static} , we observe a drop in F due to hyperfine interaction noise. In Fig. 4(b), as the ac field B_{ac} is increased, B_{static} at which $F \geq 0.98$ (B_F) decreases, thus, increasing the working range of B_{static} . In Fig. 4(c), we illustrate two curves highlighting the differences in fidelity for the NOT gate and the Hadamard gate for the same value of $B_{ac} = 0.01\text{mT}$. It appears that at a low value of B_{ac} , Hadamard gate exhibits $F \geq 0.98$ whereas NOT gate does not show high fidelity ($F \geq 0.98$) and requires a higher ac magnetic field for its operation.

In Fig. 5(a), we show F for a single qubit Hadamard gate operation as a function of B_{static} at high values of static magnetic field (few Tesla). The black (red) curve corresponds to the case when no noise (noise) is considered in the system. Both cases are taken at $B_{ac} = 0.2\text{mT}$. We found a sharp drop in F for both with and without noise cases at $B_{static} = 3.5T$. This suggests that the drop in F is not related to the decoherence but it is due to relative values of B_{static} and B_{ac} . At high values of $B_{static} \geq 5T$, we observe a drop in F due to hyperfine interaction noise. In Fig. 5(b), as the ac field B_{ac} is increased, B_{static} at which $F \geq 0.98$ also increases. Thus, increasing the working range of B_{static} . We also observe that the sharp dip in F at $B_{static} = 3.5T$ is reduced at high B_{ac} giving an extra advantage from the point of fidelity. In Fig. 5(c), we illustrate two curves highlighting the difference in fidelity for NOT gate and Hadamard gate operations for the same value of $B_{ac} =$

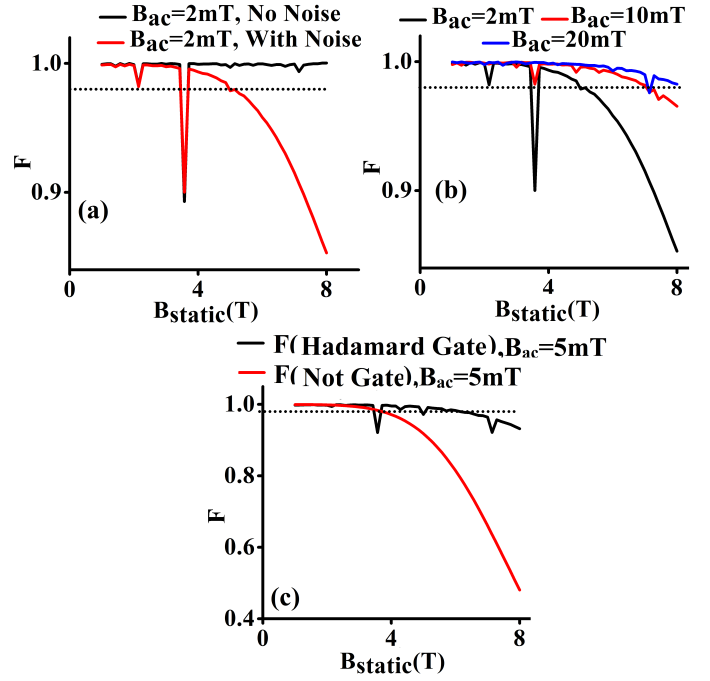


Fig. 5. (a) Fidelity vs B_{static} for hadamard gate at $B_{ac} = 2\text{mT}$, when there is no noise (black), noise (red) in the system. The peak at $B_{static} = 3.5T$ is due to B_{ac} and B_{static} values and is not due to decoherence. (b) Fidelity vs B_{static} for three values of $B_{ac} = 2\text{mT}$ (black), 10mT (red) and 20mT (blue). This shows that the fidelity drop at $B_{static} = 3.5T$ is removed at high values of B_{ac} . Moreover, at high B_{ac} a much greater range of B_{static} can be used corresponding to $F \geq 0.98$ for hadamard gate operation. (c) Fidelity comparison for NOT gate and hadamard gate operation at $B_{ac} = 5\text{mT}$.

5mT . It appears that Hadamard gate shows $F \geq 0.98$ for a greater range of B_{static} compared to the NOT gate.

C. Relation between T_2^* and B_{ac}

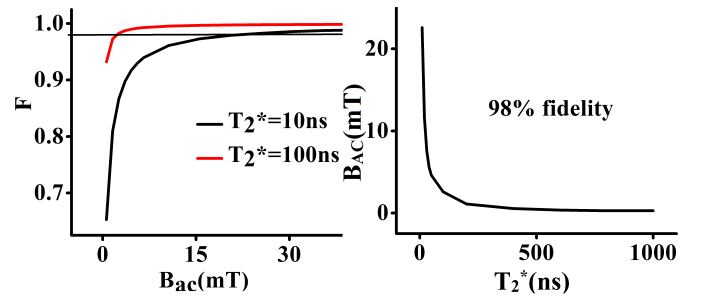


Fig. 6. (a) Fidelity vs B_{ac} for cases $\rho(0) = |\uparrow\rangle$ at two different $T_2^* = 10\text{ns}$ (black), 100ns (red) at $B_{static} = 1T$ for NOT gate. The horizontal line corresponds to $F = 0.98$ and at that point $B_{ac} = B_{AC}$. All other parameters are kept constant. (b) B_{AC} vs T_2^* depicting that at higher T_2^* , gate operation require lower B_{AC} for high fidelity (≥ 0.98) NOT gate operation.

In this subsection, we examine the relation between the ac magnetic field and gate fidelity for different values of dephasing time. We also analyze the value of ac magnetic field required to achieve high fidelity operation for a wide range of dephasing time values. Fig. 6 shows the relation of B_{ac} and T_2^* . The T_2^* is correlated with the dephasing time mentioned in Eq. 8. In Fig 6(a), we have plotted F for NOT gate operation when $\rho(0) = |\uparrow\rangle$ at $B_{static} = 1T$. This has

been done for two values of T_2^* . The dotted line corresponds to $F=0.98$. We define a quantity called B_{AC} which is the ac magnetic field when $F=0.98$ at a constant value of B_{static} . In Fig 6(b) we plot values of B_{AC} for different values of T_2^* which is required for the high fidelity gate operation. The relation shows an exponential decay highlighting that when T_2^* is relatively low (few ns) a higher B_{AC} is required. As T_2^* increases, B_{AC} is reduced and eventually it saturates and becomes independent of T_2^* .

In summary, we observe that a higher value of ac field mitigates decoherence at both high and low static magnetic field regimes. This is because raising the value of the ac magnetic field decreases the gate operation time (faster gate operation). Hence, the system gets much less time to interact with its environment, leading to lesser decoherence and better performance at both low and high static magnetic field values. We also observe that Hamdard gate implementation shows a much better response for the same set of parameters compared to the NOT gate. Finally, for a lower value of T_2^* a higher value of ac magnetic field is required for high fidelity gate operation.

IV. TOFFOLI GATE

A system of three spin qubits can be used to implement controlled-controlled NOT (CCNOT) gate or Toffoli gate, as illustrated in Fig. 7 [34]. The Toffoli gate uses two control qubits and one target qubit. Based on the states of the control qubits, the target qubit is either flipped or left unchanged. The complete Hamiltonian for three qubits Toffoli system is given by Eq. 15, where J_{12} gives exchange interaction between electrons in region R_{CL} - R_{TC} and the J_{23} is the exchange interaction for regions R_{TC} - R_{CR} (cf. Fig. 7). The middle qubit acts as the target qubit while the other two act as control qubits.

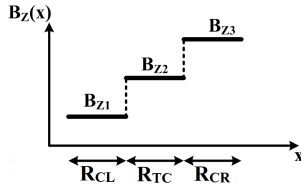


Fig. 7. Magnetic field profile for three-qubit operation. R_{CL} corresponds to the region of left control qubit, R_{TC} corresponds to the central target qubit, and R_{CR} corresponds to the region of right control qubit.

$$\begin{aligned}
H(t) = & J_{12}(\sigma_{1x}\sigma_{2x} + \sigma_{1y}\sigma_{2y} + \sigma_{1z}\sigma_{2z}) \\
& + J_{23}(\sigma_{2x}\sigma_{3x} + \sigma_{2y}\sigma_{3y} + \sigma_{2z}\sigma_{3z}) \\
& + g\mu_B B_{1z}\sigma_{1z} + g\mu_B B_{2z}\sigma_{2z} + g\mu_B B_{3z}\sigma_{3z} \quad (15) \\
& - g\mu_B B_{ac}(\cos\omega t(\sigma_{1x} + \sigma_{2x} + \sigma_{3x}) \\
& - \sin(\omega t)(\sigma_{1y} + \sigma_{2y} + \sigma_{3y}))
\end{aligned}$$

The static magnetic fields B_{z1} , B_{z2} , B_{z3} are used to create a magnetic field gradient (δB_z) where we assume that the magnetic field is constant along the length of an individual electron wave function. B_{ac} is the ac magnetic field that is used to cause state transitions at a particular frequency. When both control qubits are in the state $|\uparrow\rangle$, the state of the

target qubit is flipped; otherwise, it remains unchanged. This happens because the frequency of B_{ac} correspond to energy gap $|\uparrow_{CL}\uparrow_{TC}\uparrow_{CR}\rangle \leftrightarrow |\uparrow_{CL}\downarrow_{TC}\uparrow_{CR}\rangle$. We also assume that ($B_{z3} - B_{z2} = \delta B_{z32}$, $B_{z2} - B_{z1} = \delta B_{z21}$, $\delta B_{z32} = \delta B_{z21}$) and $J_{12}=J_{23} = J$.

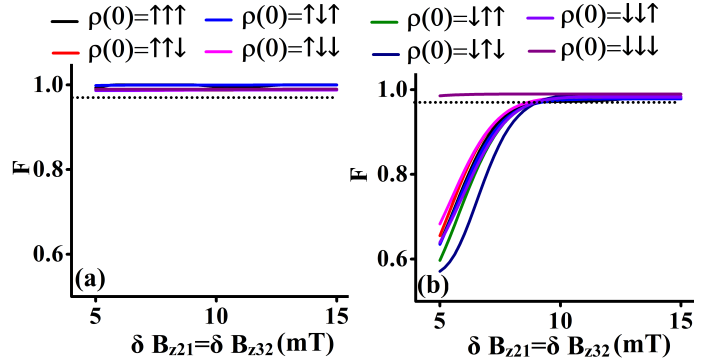


Fig. 8. (a) Fidelity vs magnetic gradient (δB_z) for $B_{ac} = 0.1mT$, $B_{z1} = 40mT$, and $J = 2.4MHz$ when no noise is considered in the system for all eight possible basis state. (b) Fidelity vs magnetic gradient (δB_z) for $B_{ac} = 0.1mT$, $B_{z1} = 40mT$, and $J = 2.4MHz$ when noise is considered in the system for all eight possible basis state. The dotted line corresponds to $F \geq 0.98$

The high fidelity Toffoli gate operation is demonstrated in Fig. 8. In our analysis, we find that a high B_{ac} gives a high-fidelity Toffoli operation where the ac field frequency corresponds to the energy gap between state $|\uparrow_{CL}\uparrow_{TC}\uparrow_{CR}\rangle \leftrightarrow |\uparrow_{CL}\downarrow_{TC}\uparrow_{CR}\rangle$. The gate fidelity is observed to be high ($\geq 98\%$) for cases when $\rho(0) = |\uparrow_{CL}\uparrow_{TC}\uparrow_{CR}\rangle$ or when $\rho(0) = |\uparrow_{CL}\downarrow_{TC}\uparrow_{CR}\rangle$. However, in all the other cases, fidelity will in fact reduce with a high ac field. For example: when $\rho(0) = |\downarrow_{CL}\uparrow_{TC}\uparrow_{CR}\rangle$, the state should remain unchanged, however due to high B_{ac} we see oscillation of small magnitude which results in $F \leq 0.98$. On the other hand, if the B_{ac} is small, we find that the resonant state shows $F \leq 0.98$. So it becomes a challenge to identify the B_{ac} which shows high fidelity for all the basis states. From Fig. 8, we find that when $B_{z1}=40$ mT, $J = 2.4MHz$, $B_{ac} = 0.1mT$ and $\delta B_z \geq 12mT$, we obtain $F \geq 0.98$.

From a practical standpoint, it is difficult to achieve gradients of more than a few mT/nm through micromagnets [35]. Therefore, practical Toffoli implementation may not possible at the high magnetic field gradients (few T/nm) where phononic noise becomes a dominant source of decoherence. Owing to this, high-fidelity universal gate implementation is limited by multi-qubit operation rather than the single qubit based gates. Putting together the single qubit gates and Toffoli gate operation, we conclude that $B_{ac}=0.1$ mT is ideal for high-fidelity universal gate implementation.

V. CONCLUSION

In this work, we have presented a scheme for implementing high-fidelity universal quantum gates based on quantum dots in presence of hyperfine interaction noise and charge noise due to phonons. We estimate the parameter range of static and ac magnetic fields corresponding to high-fidelity ($> 98\%$) gate operations in noisy. In addition, we find that the parameter

range of the gate operations is limited by the initial qubit state having the least energy in high static magnetic field regime. On the other hand, in low static magnetic field regime, the range is limited by initial qubit state having the least energy gap with respect to all other states. We also examine the interplay between the ac magnetic field and decoherence time in single qubit gates that gives us interesting insights about the magnetic field value to be used in a gate operation. We also identify a common parameter regime for Hadamard and Toffoli gate implementations. In future, we plan to devise noise cancellation techniques based on dynamical decoupling pulse sequences and gradient ascent pulse engineering (GRAPE) technique that can further improve the gate fidelity and possibly increase the operating range of these parameters and make the quantum gates more resilient thus reducing the error correction overhead. The framework presented in this work can be extended to a larger system (i.e. a multi-qubit quantum processor) to execute various gate operations and would be helpful in understanding the execution of quantum algorithms using quantum dot-based spin qubits.

REFERENCES

- [1] D. Loss and D. P. DiVincenzo, "Quantum computation with quantum dots," *Physical Review A*, vol. 57, no. 1, p. 120, 1998.
- [2] F. H. Koppens, C. Buizert, K.-J. Tielrooij, I. T. Vink, K. C. Nowack, T. Meunier, L. Kouwenhoven, and L. Vandersypen, "Driven coherent oscillations of a single electron spin in a quantum dot," *Nature*, vol. 442, no. 7104, pp. 766–771, 2006.
- [3] B. M. Maune, M. G. Borselli, B. Huang, T. D. Ladd, P. W. Deelman, K. S. Holabird, A. A. Kiselev, I. Alvarado-Rodriguez, R. S. Ross, A. E. Schmitz *et al.*, "Coherent singlet-triplet oscillations in a silicon-based double quantum dot," *Nature*, vol. 481, no. 7381, pp. 344–347, 2012.
- [4] M. Veldhorst, J. Hwang, C. Yang, A. Leenstra, B. de Ronde, J. Dehollain, J. Muhonen, F. Hudson, K. M. Itoh, A. Morello *et al.*, "An addressable quantum dot qubit with fault-tolerant control-fidelity," *Nature nanotechnology*, vol. 9, no. 12, pp. 981–985, 2014.
- [5] M. Veldhorst, C. Yang, J. Hwang, W. Huang, J. Dehollain, J. Muhonen, S. Simmons, A. Laucht, F. Hudson, K. M. Itoh *et al.*, "A two-qubit logic gate in silicon," *Nature*, vol. 526, no. 7573, pp. 410–414, 2015.
- [6] D. M. Zajac, A. J. Sigillito, M. Russ, F. Borjans, J. M. Taylor, G. Burkard, and J. R. Petta, "Resonantly driven cnot gate for electron spins," *Science*, vol. 359, no. 6374, pp. 439–442, 2018.
- [7] M. Russ, D. M. Zajac, A. J. Sigillito, F. Borjans, J. M. Taylor, J. R. Petta, and G. Burkard, "High-fidelity quantum gates in si/sige double quantum dots," *Physical Review B*, vol. 97, no. 8, p. 085421, 2018.
- [8] D. Zajac, T. Hazard, X. Mi, K. Wang, and J. R. Petta, "A reconfigurable gate architecture for si/sige quantum dots," *Applied Physics Letters*, vol. 106, no. 22, p. 223507, 2015.
- [9] J. R. Petta, A. C. Johnson, J. M. Taylor, E. A. Laird, A. Yacoby, M. D. Lukin, C. M. Marcus, M. P. Hanson, and A. C. Gossard, "Coherent manipulation of coupled electron spins in semiconductor quantum dots," *Science*, vol. 309, no. 5744, pp. 2180–2184, 2005.
- [10] R. Hanson, L. P. Kouwenhoven, J. R. Petta, S. Tarucha, and L. M. Vandersypen, "Spins in few-electron quantum dots," *Reviews of modern physics*, vol. 79, no. 4, p. 1217, 2007.
- [11] D. Zajac *et al.*, "Single electron spin qubits in silicon quantum dots," Ph.D. dissertation, Princeton University, 2018.
- [12] M. A. Nielsen and I. L. Chuang, "Quantum computation and quantum information," *Phys. Today*, vol. 54, no. 2, p. 60, 2001.
- [13] A. W. Harrow, B. Recht, and I. L. Chuang, "Efficient discrete approximations of quantum gates," *Journal of Mathematical Physics*, vol. 43, no. 9, pp. 4445–4451, 2002.
- [14] J. M. Taylor, *Hyperfine interactions and quantum information processing in quantum dots*, 2006, vol. 67, no. 12.
- [15] S. Amasha, K. MacLean, I. P. Radu, D. Zumbühl, M. Kastner, M. Hanson, and A. Gossard, "Electrical control of spin relaxation in a quantum dot," *Physical review letters*, vol. 100, no. 4, p. 046803, 2008.
- [16] A. V. Khaetskii and Y. V. Nazarov, "Spin-flip transitions between zeeman sublevels in semiconductor quantum dots," *Physical Review B*, vol. 64, no. 12, p. 125316, 2001.
- [17] P. San-Jose, G. Zarand, A. Shnirman, and G. Schön, "Geometrical spin dephasing in quantum dots," *Physical review letters*, vol. 97, no. 7, p. 076803, 2006.
- [18] F. Marquardt and V. A. Abalmassov, "Spin relaxation in a quantum dot due to nyquist noise," *Physical Review B*, vol. 71, no. 16, p. 165325, 2005.
- [19] M. Borhani, V. N. Golovach, and D. Loss, "Spin decay in a quantum dot coupled to a quantum point contact," *Physical Review B*, vol. 73, no. 15, p. 155311, 2006.
- [20] L. P. Kouwenhoven, C. M. Marcus, P. L. McEuen, S. Tarucha, R. M. Westervelt, and N. S. Wingreen, "Electron transport in quantum dots," in *Mesoscopic electron transport*. Springer, 1997, pp. 105–214.
- [21] C. Simmons, M. Thalakulam, N. Shaji, L. J. Klein, H. Qin, R. Blick, D. Savage, M. Lagally, S. Coppersmith, and M. Eriksson, "Single-electron quantum dot in si/si ge with integrated charge sensing," *Applied Physics Letters*, vol. 91, no. 21, p. 213103, 2007.
- [22] L. C. Camenzind, L. Yu, P. Stano, J. D. Zimmerman, A. C. Gossard, D. Loss, and D. M. Zumbühl, "Hyperfine-phonon spin relaxation in a single-electron gas quantum dot," *Nature communications*, vol. 9, no. 1, pp. 1–6, 2018.
- [23] A. Alcalde, C. Romano, and G. Marques, "Spin relaxation rates in quantum dots: Role of the phonon modulated spin-orbit interaction," *Solid state communications*, vol. 148, no. 5-6, pp. 255–258, 2008.
- [24] F. A. Zwanenburg, A. S. Dzurak, A. Morello, M. Y. Simmons, L. C. Hollenberg, G. Klimeck, S. Rogge, S. N. Coppersmith, and M. A. Eriksson, "Silicon quantum electronics," *Reviews of modern physics*, vol. 85, no. 3, p. 961, 2013.
- [25] M. Eriksson, S. Coppersmith, and M. Lagally, "Semiconductor quantum dot qubits," *MRS bulletin*, vol. 38, no. 10, pp. 794–801, 2013.
- [26] D. Aharonov, "A simple proof that toffoli and hadamard are quantum universal," *arXiv preprint quant-ph/0301040*, 2003.
- [27] R. Vilmart, "Completeness of sum-over-paths for toffoli-hadamard and the clifford hierarchy," *arXiv preprint arXiv:2205.02600*, 2022.
- [28] S. Mehl and D. P. DiVincenzo, "Noise analysis of qubits implemented in triple quantum dot systems in a davies master equation approach," *Physical Review B*, vol. 87, no. 19, p. 195309, 2013.
- [29] D. Paget, G. Lampel, B. Sapoval, and V. Safarov, "Low field electron-nuclear spin coupling in gallium arsenide under optical pumping conditions," *Physical review B*, vol. 15, no. 12, p. 5780, 1977.
- [30] F. Koppens, K. Nowack, and L. Vandersypen, "Spin echo of a single electron spin in a quantum dot," *Physical Review Letters*, vol. 100, no. 23, p. 236802, 2008.
- [31] L. v. Dommelen, "Nuclear Magnetic Resonance." [Online]. Available: https://web1.eng.famu.fsu.edu/~dommelen/quantum/style_a/nmr.html
- [32] M. Le Bellac *et al.*, *A short introduction to quantum information and quantum computation*. Cambridge University Press, 2006.
- [33] Y. Tiwari, T. Sarkar, and V. S. Poonia, "Effect of ac magnetic field on single qubit gate operation in noisy environment," in *2022 IEEE 22nd International Conference on Nanotechnology (NANO)*. IEEE, 2022, pp. 375–378.
- [34] M. Gullans and J. Petta, "Protocol for a resonantly driven three-qubit toffoli gate with silicon spin qubits," *Physical Review B*, vol. 100, no. 8, p. 085419, 2019.
- [35] J. Yoneda, T. Otsuka, T. Takakura, M. Pioro-Ladrière, R. Brunner, H. Lu, T. Nakajima, T. Obata, A. Noiri, C. J. Palmstrøm *et al.*, "Robust micromagnet design for fast electrical manipulations of single spins in quantum dots," *Applied Physics Express*, vol. 8, no. 8, p. 084401, 2015.